Title

Voxel-based morphometric analyses of the brain in children and adolescents prenatally exposed to alcohol

Journal

Neuroreport, 12(3)

ISSN

0959-4965

Authors

Sowell, Elizabeth R

Thompson, Paul M

Mattson, Sarah N

et al.

Publication Date

2001-03-01

DOI

10.1097/00001756-200103050-00018

Peer reviewed

Voxel-based morphometric analyses of the brain in children and adolescents prenatally exposed to alcohol

Elizabeth R. Sowell,[CA] Paul M. Thompson, Sarah N. Mattson,[1] Kevin D. Tessner, Terry L. Jernigan,[2] Edward P. Riley[1] and Arthur W. Toga

University of California, Los Angeles, Department of Neurology, Laboratory of Neuro Imaging, 710 Westwood Plaza, Room 4-238, Los Angeles, CA 90095-1769; [1]Center for Behavioral Teratology, San Diego State University; [2]Department of Veterans Affairs Medical Center and Departments of Psychiatry and Radiology, University of California, San Diego, School of Medicine, USA

[CA]Corresponding Author

Received 21 November 2000; accepted 1 December 2000

Children of mothers who abuse alcohol during pregnancy can suffer varying degrees of neurological abnormality, cognitive impairment, and behavioral problems, and in the worst case, are diagnosed with fetal alcohol syndrome (FAS). The purpose of the present study was to localize brain abnormalities in a group of children and adolescents prenatally exposed to alcohol using high resolution, 3D structural MRI data and whole-brain voxel-based morphometry (VBM). Data were collected for 21 children and adolescents with histories of prenatal alcohol exposure (ALC) and 21 normally developing individuals. Statistical parametric maps revealed abnormalities most prominent in the left hemisphere perisylvian cortices of the temporal and parietal lobes where the ALC patients tended to have too much gray matter and not enough white matter. These results provide further support for dysmorphology in temporo-parietal cortices above and beyond the overall microcephaly that results from severe prenatal alcohol exposure. *NeuroReport* 12:515–523 © 2001 Lippincott Williams & Wilkins.

Key words: Fetal alcohol syndrome; Imaging; Perisylvian cortex; Prenatal alcohol exposure; MRI

INTRODUCTION

Few neuroimaging studies in the literature have focused on fetal alcohol syndrome (FAS), despite its relatively common occurrence (~0.33/1000 [1]), and the well-documented teratogenic effects of prenatal exposure to alcohol described with animal models [2]. Microcephaly and neuronal migration abnormalities are among the most commonly observed anomalies in the few autopsy studies in the literature, and callosal and cerebellar vermal abnormalities have also been reported [3]. *In vivo* MRI studies have confirmed microcephaly [4–7], callosal area [8], basal ganglia [4–6], mesial temporal lobe [9] and cerebellar vermal abnormalities [10] in FAS patients.

In a recent report, we described abnormalities in the shape and location of the corpus callosum that were confined to posterior splenium and isthmus regions in children and adolescents prenatally exposed to alcohol (ALC patients) [7]. This would suggest that more distal cortices connected by the posterior regions of the corpus callosum might be more severely affected in ALC patients while the more anterior cortices connected via the anterior body and genu regions of the corpus callosum remain less affected. This hypothesis is consistent with volumetric studies of some of the same patients studied here that reveal disproportionate volume reductions in white matter relative to gray matter, most prominently in parietal regions [6] (those probably innervated by posterior callosal fibers [11]). While these studies have provided some converging evidence for regional specificity of brain abnormalities as a result of prenatal exposure to alcohol, the spatial localization of dysmorphology has been assessed only at the relatively gross level of cortical lobes and subcortical structures [6].

The purpose of the present study was to localize brain abnormalities in a group of children and adolescents prenatally exposed to alcohol using whole-brain voxel-based morphometry (VBM). Using these methods, the whole brain can be analyzed at once without the labor-intensive slice-by-slice region definition required of volumetric studies. Additionally, brain regions without clear gyral or structural boundaries (i.e. white matter) can also be assessed with VBM. Similar methods have been used to study other developmental disorders such as autism [12] and childhood-onset schizophrenia [13].

Given that posterior callosal regions are abnormal in these ALC patients [7], and volumetric studies have shown abnormalities somewhat specific to the parietal lobes [6], we predicted that we would see more abnormalities in the

posterior temporo-parietal junction in the ALC patients and that the abnormalities would be better localized than in prior volumetric studies.

MATERIALS AND METHODS

Subjects: Twenty-one children, adolescents, and young adults with prenatal alcohol exposure who were between the ages of 8 and 22 years (mean $\pm$ s.d. 13 ± 4 years; 11 female, two left handed) were studied with MRI. All alcohol-exposed children were evaluated by a dysmorphologist, and all of the children and young adults had histories of heavy prenatal alcohol exposure. Results from neuropsychological testing in these subjects are presented elsewhere [14,15]. Fourteen had the characteristic facial appearance [16] that allowed for a diagnosis of fetal alcohol syndrome (FAS; mean age 12.6 ± 4 years, eight female, one left handed). Seven other subjects did not have the facial features to warrant a diagnosis of FAS (mean age 13 ± 3.8 years, three female, one left handed) but were exposed to large quantities of alcohol *in utero* (prenatally exposed to alcohol; PEA). The alcohol-exposed subjects were combined for the basic analyses, though some *post-hoc* analyses were conducted with the 14 FAS and seven PEA subjects in separate groups. Mothers of all 21 ALC subjects were known from medical, personal, or relative reports to be alcohol abusers and to have continued drinking heavily during their pregnancies. Specifics about the amount of alcohol consumed during pregnancy were not available.

Twenty-one normal children, adolescents and young adults between 8 and 25 years were studied as a comparison group (mean age 13.5 ± 5 years, 12 female; all right handed). All child and adolescent subjects were recruited as normal controls for a large, multidisciplinary neurodevelopmental research center or for the Center for Behavioral Teratology, both in San Diego. Each subject was screened for neurological impairments and for any history of learning disability, or developmental delay. Informed consent was obtained from all children and their parents. The young adult subjects were recruited as normal controls for neuropsychiatric studies of adult patient populations. These subjects were thoroughly screened for medical, neurological, and psychiatric disorders, and informed consent was obtained from each subject.

The subjects studied here (ALC and control subjects) are the same patients examined earlier in our report on callosal abnormalities [7]. These subjects (ALC patients and controls) also comprise a subset of a larger group studied earlier with volumetric methods [6].

Imaging protocol: MRI was performed with a 1.5 T magnet (Signa: General Electric, Milwaukee). A gradient-echo (SPGR) T1-weighted series was collected for each subject with TR = 24 ms, TE = 5 ms, NEX = 2, flip angle = 45°, field of view 24 cm, section thickness 1.2 mm, no gaps (shown in Fig. 1), with an imaging time of 19 min.

Image Analysis: Image preprocessing methods are described in detail in an earlier report [17], and are briefly summarized here. First, image data was resliced into a standard orientation by trained operators tagging 10 standardized anatomical landmarks in each subject's image data set that corresponded to the same 10 anatomical landmarks defined in an average brain atlas (ICBM-305) [18]. This reslicing step was performed only to provide image analysts with a standard view of the brain, making it easier to apply standardized rules for defining cerebral and non-cerebral regions. A 3-dimensional spatial filter was then applied to each brain volume to remove low frequency changes, or drifts in signal value across the volume that commonly occur as a result of magnet inhomogeneity artifact. This step is important for accurate gray matter/white matter tissue classification. Semi-automated tissue segmentation was then conducted for each spatially filtered volume data set to classify voxels based on signal value as most representative of gray matter, white matter, or cerebrospinal fluid (CSF). A detailed discussion of the reliability and validity of the tissue segmentation protocol is presented in Sowell *et al.* [17]. A sample tissue segmented image slice can be viewed in Fig. 1. Tissue classified images were then used to aid in creating a mask of the brain where the CSF around the outer edge of the cortex (in most places) could be used as a predefined border between brain and skull. Using the brain mask, non-brain tissue and cerebellar structures were then removed from the image volumes.

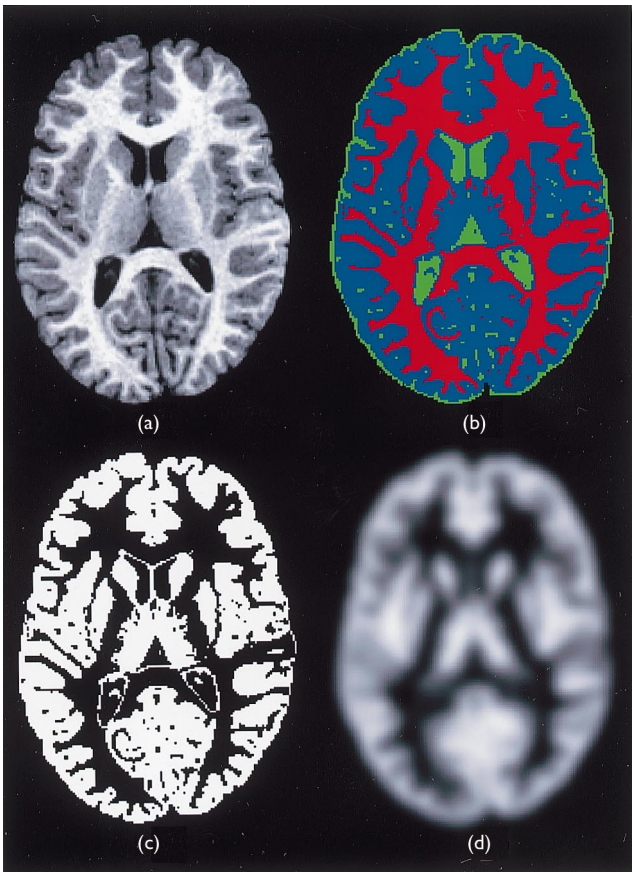

Fig. 1. Representative axial slices from one individual subject illustrating the gray-scale T1-weighted protocol (**a**), tissue segmentation where voxels most representative of gray matter are shown in blue, white matter in red, and CSF in green (**b**), binarized image where all gray matter voxels are labeled 1, and all non-gray matter voxels are labeled 0 (**c**), and gray matter binary image smoothed with an 8 mm FWHM kernel (**d**).

The tissue classified supratentorial volume from each subject was scaled into a standard space using an automated 12 parameter linear transformation [19]. This procedure, in effect, removes variability due to head size differences. After spatial normalization, the segmented volumes were binarized to include only voxels that segmented as gray matter (blue regions in Fig. 1) as one data set, and voxels that segmented as white matter (red regions in Fig. 1), as a second data set. Both were imported into the SPM99 software [20]. The spatially normalized gray and white matter maps were smoothed with an 8 mm FWHM isotropic Gaussian kernel to create a spectrum of gray or white matter intensities needed for the statistical analyses (see sample smoothed gray matter image in Fig. 1).

Statistical analyses: Previous reports have shown a similar pattern of dysmorphology in the FAS and PEA groups [6,7]. Thus to maximize statistical power, the planned analyses were conducted with all 21 ALC patients.

Volumetric measures of total supratentorial intracranial volume (SIV; in native space prior to scaling), total gray matter, total white matter, and total CSF were assessed for group differences with *t*-tests. Next, total gray matter, total white matter, and total CSF were assessed for group differences in three separate simultaneous multiple regression analyses where both group membership and total SIV were used to predict the volume measure of interest (i.e. gray matter, white matter or CSF). In this way, it could be determined how much of the group difference in each tissue type was accounted for by generalized brain volume reduction.

We used VBM to localize morphological differences between the 21 ALC subjects and the 21 controls (using SPM99 software [20]). VBM analyses, which allow assessment of group differences at every point in the brain, result in statistical parametric maps (SPMs) showing a *t*-statistic at every voxel. Inferences about the localization and regional specificity of brain tissue abnormalities (gray matter or white matter) can be made based on the resultant maps. Here, two basic analyses were conducted: one contrast assessing localization of gray matter differences between ALC and control groups and the other contrast assessing localization of white matter differences between ALC and control groups. For both analyses, we required that each voxel be different between groups using a threshold of $p = 0.0001$ to be considered significant. Additionally, only clusters extending to $\geqslant 50$ contiguous voxels (significant at $p = 0.0001$) were considered significant. These thresholds were chosen because they seemed to best characterize expected structural differences between groups and are similar to those we have used in previous studies [17,21].

In order to assess the validity and overall statistical significance of the gray and white matter SPMs, the ALC subjects and controls were randomly assigned to groups for 20 new analyses (for each tissue type) from which the results (using the same voxel threshold of $p = 0.0001$ and extent threshold of $\geqslant 50$ voxels as the group comparisons) were tabulated. In these analyses, we counted the number of significant clusters revealed in the group difference analyses and compared that number to the number of significant clusters revealed in the randomized SPMs. This randomization approach has been reported previously as a method for protecting against false positive errors given the large number of multiple comparisons required for VBM [13,17,21,22]. Randomization is essential in this type of analysis (i.e. where structural imaging data are assessed). This is because false positive errors have an unacceptably high rate when using SPM99's correction for multiple comparisons which relies on the theory of Gaussian random fields [23,24]. The number of false positives varies depending on the required cluster size, extent threshold and the spatial smoothness of the residuals of the statistical model [23]. Thus, while a recent methodological report has shown that the use of a theoretical null distribution is inappropriate in VBM analyses that use SPM99's correction for multiple comparisons [23] this is not the case when one relies on randomization, as we did here, to protect against type 1 error.

Post hoc SPM analyses were conducted to assess for gray matter differences between the 14 FAS patients and control subjects, and then between the seven PEA patients and control subjects. This was in order to determine whether differences in the patterns of tissue distribution occurring in individuals with milder symptoms of prenatal alcohol exposure could also be detected with VBM.

RESULTS

Volume measures: All volume measures reported here are for supratentorial regions computed in native space (before spatial normalization). Significant group differences were observed for total intracranial volume ($t = 4.5$, $p < 0.001$), total gray matter volume ($t = 2.8$, $p < 0.01$), total white matter volume ($t = 4.8$, $p < 0.001$), and total CSF volume ($t = 3.5$, $p < 0.01$). In all cases, the ALC patients had smaller volumes than the controls. Results from the simultaneous multiple regression analyses revealed a partial correlation between group membership and the measure of total white matter that was no longer significant when SIV was used as an additional predictor. The same was true for CSF. This suggests that group differences in these measures are not independent of overall SIV reduction. The partial correlation coefficient for gray matter, however, was still at trend level significance in predicting group membership ($\beta = 0.16$, $p = 0.08$) even when the highly significant effects of SIV were controlled ($\beta = 0.98$, $p < 0.001$). Notably, the group effect indicates that relative to the overall reduced brain volume, the ALC patients may have too much gray matter.

Gray matter SPM: The SPM of the gray matter differences (voxel threshold $p < 0.0001$) between the two groups shows 17 significant clusters of $\geqslant 50$ significant voxels with a large cluster in the left posterior temporo-parietal cortex that tends to segment as gray matter in the ALC group and not gray matter (e.g. white matter or CSF) in the controls. The SPM can be seen mapped onto the spatially normalized surface rendering of one individual's brain in Fig. 2, and mapped onto orthogonal slices of the same individual in Fig. 3. Note that only clusters near the surface of the brain can be seen on the surface rendering in Fig. 2, and deeper clusters are mapped onto orthogonal slices shown in Fig. 3. No significant clusters were observed in the opposite contrast for regions of gray matter in the controls

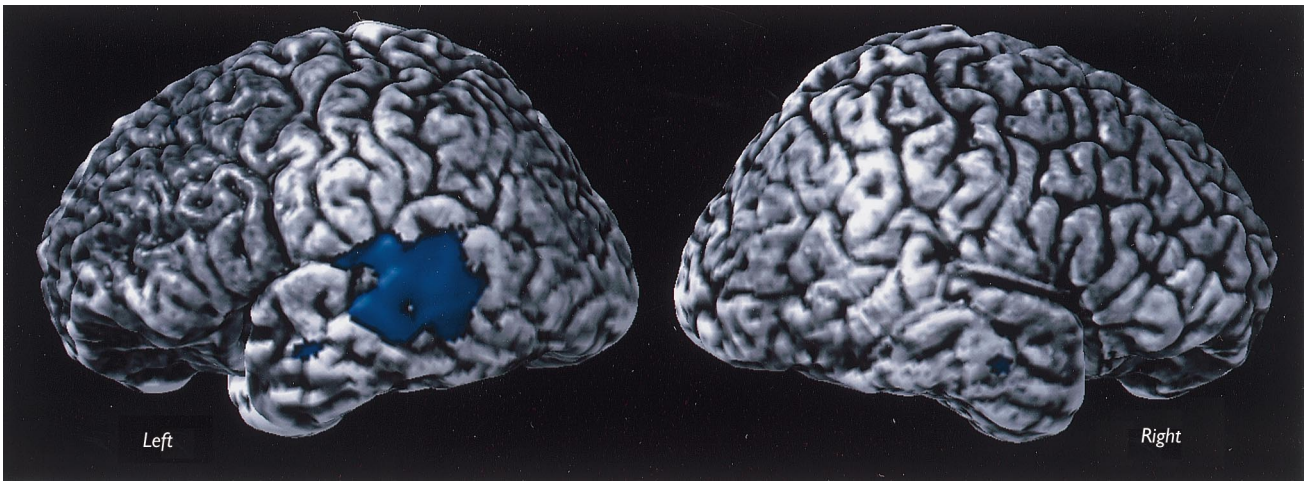

Fig. 2. Gray matter SPM showing regions that tend to segment as gray matter in the ALC subjects and non-gray matter in the controls mapped onto a surface rendering of one representative subject's brain. Note that only clusters near the surface of the brain are shown on the surface rendering and clusters deeper within the brain can be seen mapped onto the orthogonal slices.

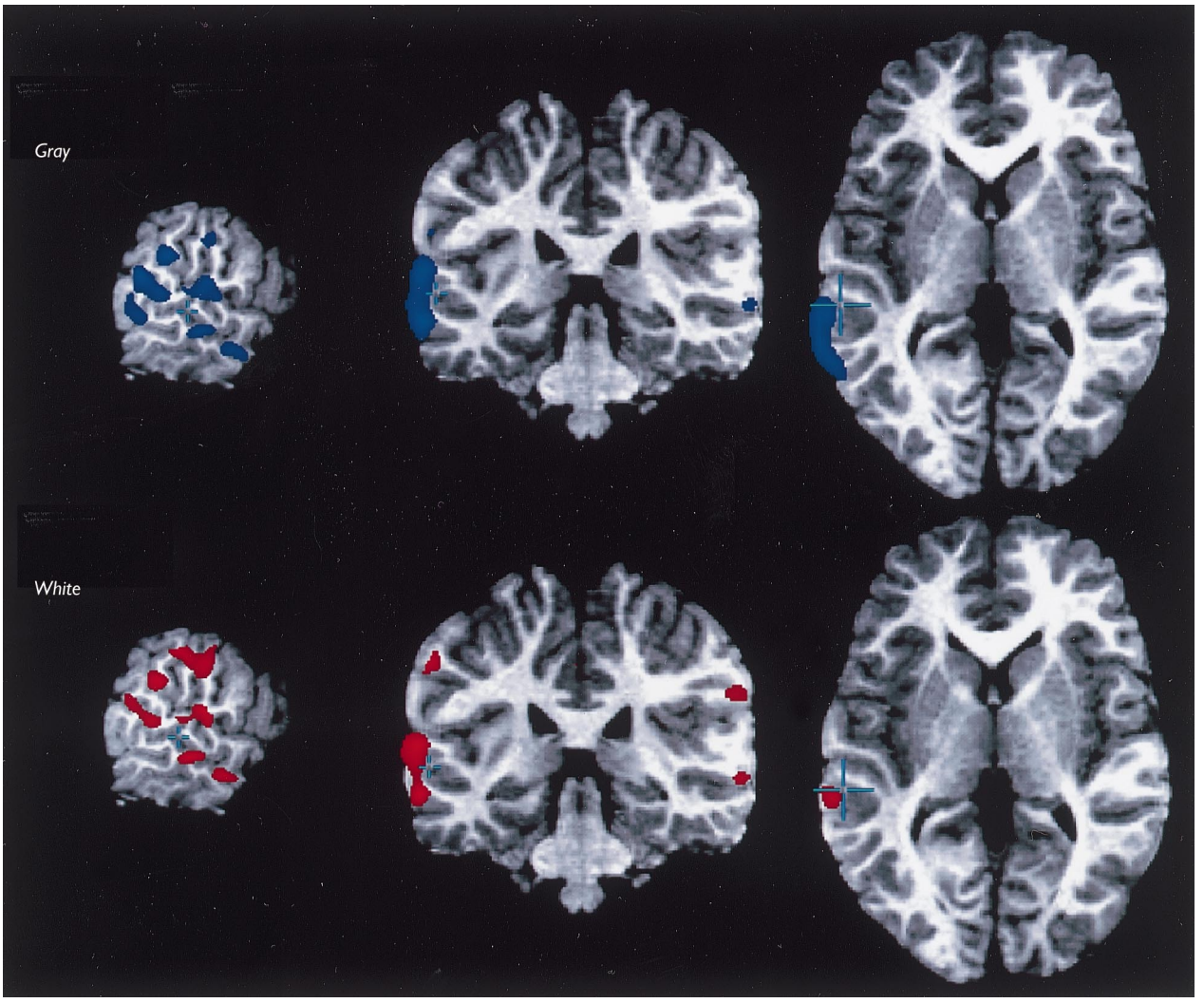

Fig. 3. Gray matter SPM mapped onto three orthogonal slices of one individual subject's brain. In blue are regions that segmented as gray matter in the ALC patients and non-gray matter in the controls (Top), white matter SPM where regions in red represent voxels that segment as white matter in the controls and non-white matter in the ALC patients.

Table 1. Talairach coordinates and z-scores for the most significant voxel in each of the clusters, and volumes for all significant clusters in the gray and white matter SPMs.

Gray matter SPM				White matter SPM			
Cluster No.	Cluster Size	z-score	x,y,z (mm)	Cluster No.	Cluster Size	z-score	x,y,z (mm)
1	10516	−5.82	−63,−30,−2	1	4872	−5.54	−62,−30,−2
2	275	−5.01	59,−27,17	2	262	−5.18	59,−27,17
3	69	−4.62	30,−27,65	3	1061	−4.81	−1,26,48
4	423	−4.57	−58,−14,−12	4	534	−4.81	−59,−43,33
5	63	−4.33	52,26,17	5	1069	−4.57	−58,−35,48
6	272	−4.29	−5,27,46	6	202	−4.43	−2,−40,45
7	116	−4.21	−58,−22,42	7	57	−4.36	30,−27,65
8	305	−4.17	−29,35,56	8	77	−4.29	−20,−65,45
9	54	−4.14	−20,−65,45	9	64	−4.25	−13,40,35
10	104	−4.14	64,−35,3	10	82	−4.24	−48,−2,59
11	80	−4.11	63,−11,−17	11	103	−4.18	63,−35,2
12	64	−4.06	−8,44,22	12	114	−4.13	39,29,31
13	63	−4.04	57,−7,37	13	53	−4.09	29,−16,−14
14	113	−4.01	47,33,32	14	143	−4.08	−13,−71,−3
15	53	−4.00	59,−33,35	15	115	−4.08	−27,7,−28
16	168	−3.95	4,−44,16	16	85	−4.07	44,49,−7
17	118	−3.95	−56,−52,−13	17	86	−4.06	63,−27,47
				18	218	−4.06	62,−33,35
				19	103	−4.04	−32,−74,−11
				20	81	−4.04	−3,−50,29
				21	75	−4.02	55,−8,37
				22	94	−4.02	−64,−47,1
				23	75	−4.00	−56,−13,38
				24	96	−3.99	−1,43,20
				25	67	−3.90	60,−15,47

that segment as non-gray matter in the ALC group (with voxel threshold $p = 0.0001$, $\geqslant 50$ significant voxels). These data are presented in Table 1 where the Talairach coordinate [25] and z-score for the most significant voxel in each of the 17 clusters are reported in addition to the number of significant voxels in each cluster.

Permutation tests were conducted to confirm the significance of group differences between the ALC subjects and controls. In 20 new tests where subjects were randomly assigned to groups and the same voxel threshold and cluster size were used as in the group test, an average of 0.3 significant clusters occurred by chance. The maximum number of significant clusters in any one randomized gray matter SPM was 1, compared with the 17 significant

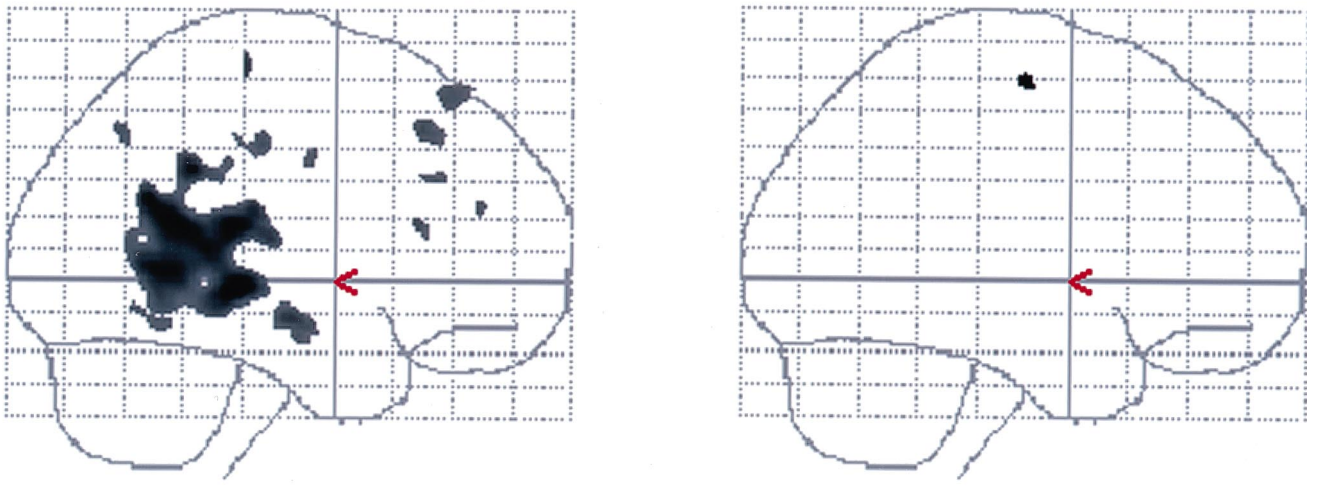

Fig. 4. SPMs for gray matter group difference (left) and for gray matter where subjects were randomly assigned to groups (right). The random map shows a single, small, circumscribed, cluster that occurred by chance which is quite dissimilar to the large regionally specific cluster observed in the real group difference gray matter SPM.

clusters in the group comparison ($p < 0.05$, permutation test). A sample gray matter random SPM can be seen in Fig. 4 in relation to the SPM for the group difference.

White matter SPM: The SPM of the white matter differences (voxel threshold $p = 0.0001$) between the two groups is shown mapped onto the spatially normalized surface rendering of one individual's brain in Fig. 5, and mapped onto orthogonal slices of the same individual in Fig. 3. The white matter SPM has 25 significant clusters of ≥ 50 significant voxels with the largest cluster in the left posterior temporo-parietal region, spatially corresponding to the largest cluster observed in the gray matter SPM. These voxels tended to segment as white matter in the controls and not white matter (e.g. gray matter or CSF) in the ALC group. Again, no significant clusters were observed in the opposite contrast. Scatterplots of the signal value by group effect for the most significant voxel in the temporal lobe region for the gray and white matter SPMs can be seen in Fig. 6. Details for the 25 significant clusters are presented in Table 1.

Permutation tests using the same thresholds as the group test revealed an average of 0.7 significant clusters occurring by chance in the 20 random white matter SPMs. The maximum number of significant clusters in any one randomized SPM was four compared to the 25 significant clusters in the group comparison ($p < 0.05$, permutation test).

***FAS* vs *control* SPM:** The SPM of the gray matter differences (voxel threshold $p < 0.0001$) between the 14 FAS subjects and the 21 controls reveals 30 clusters of ≥ 50 significant voxels. The pattern is very similar to that observed for the combined ALC group where the largest cluster is in the left posterior temporo-parietal cortex. Again, this region tends to segment as gray matter in the FAS group and not gray matter in the controls. The SPM can be seen mapped onto the spatially normalized surface rendering of one individual's brain and mapped onto orthogonal slices of the same individual in Fig. 7 (shown in red). Note the overlap with the total ALC group *vs* control differences (mapped on the same brain surface in green) is almost complete, with the FAS *vs* control comparison yielding slightly larger clusters centered within ~4 mm of the same peak voxel (e.g. Talairach coordinates −63, −30, −2 for all ALC patients *vs* controls and coordinates −65, −33, −4 for the FAS *vs* control comparison).

***PEA* vs *control* SPM:** The SPM of gray matter differences between the seven PEA subjects and the 21 controls revealed 16 significant clusters (voxel threshold $p = 0.001$) with ≥ 50 significant voxels, one of which was in the left temporo-parietal region within ~2 mm of the same peak voxel (Talairach coordinates −61, −29, −3) as the other two gray matter SPMs (i.e. ALC *vs* control and FAS vs. control). The results were somewhat less robust (note the lower voxel threshold used here), either because of a smaller sample size, or because the PEA patients are less severely affected than the FAS patients. The SPM can be seen mapped onto the spatially normalized surface rendering of one individual's brain and mapped onto orthogonal slices of the same individual in Fig. 7 (shown in blue). Again, there is considerable overlap of the clusters in the PEA *vs* control comparison as observed in the other two gray matter SPMs.

DISCUSSION

Voxel-by-voxel analyses of gray matter and white matter tissue maps reveal regional brain abnormalities in the ALC subjects that are generally consistent with our *a priori* hypotheses, and consistent with the brain imaging literature on prenatal alcohol exposure. Abnormalities are found primarily in a large region of the posterior temporo-parietal cortex in the left hemisphere where ALC patients tend to have too much gray matter and too little white matter. Interestingly, posterior callosal fibers connect temporo-parietal cortices between the two hemispheres and this is the same region of the corpus callosum found to be abnormal in these subjects in an earlier study [7]. Volume reductions of gray and white matter in the parietal lobes

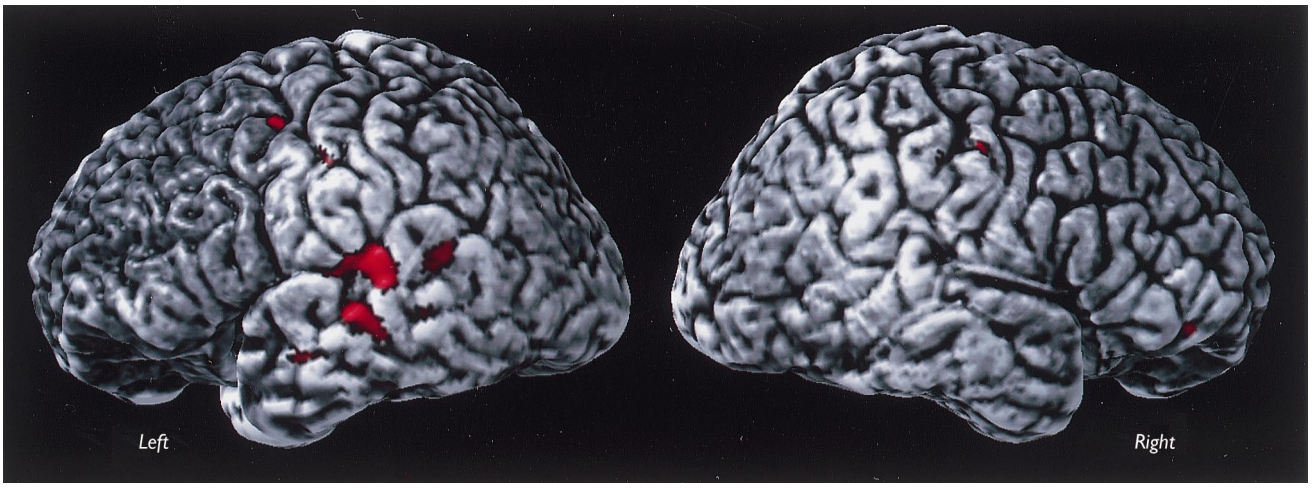

Fig. 5. White matter SPM showing regions that tend to segment as white matter in the controls and non-white matter in the ALC subjects mapped onto a surface rendering of one representative subject's brain.

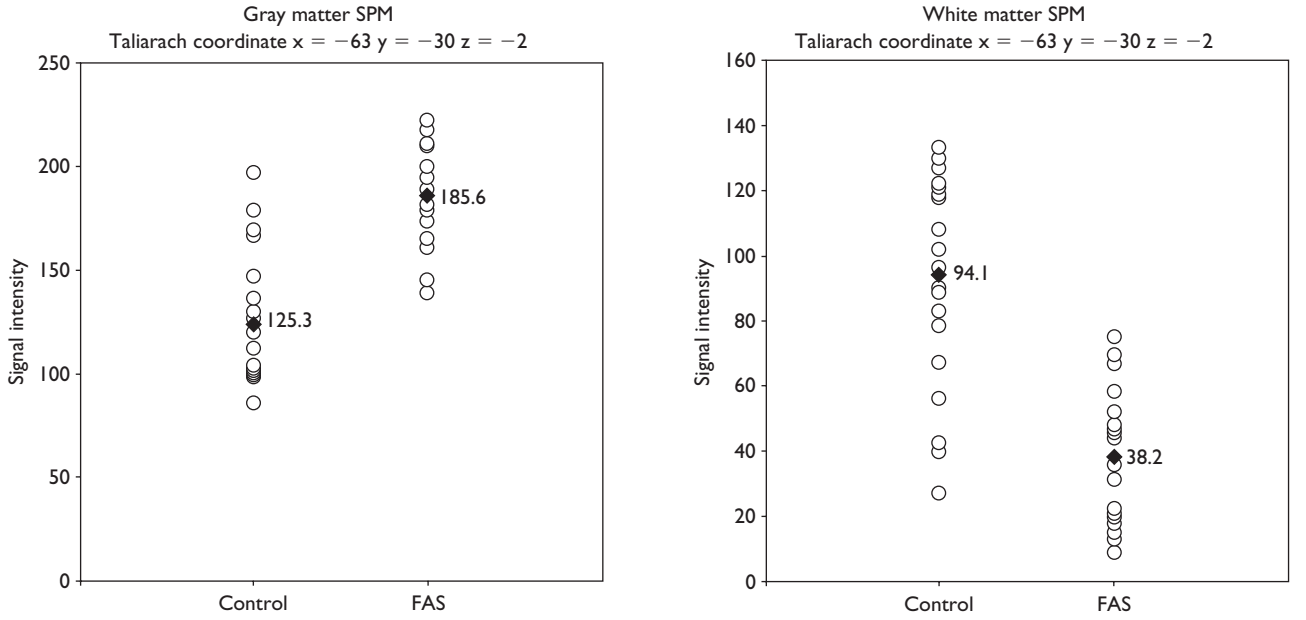

Fig. 6. Scatterplots representing the group effect for gray matter signal differences (left) and white matter differences (right) in the left temporal lobe at Talairach coordinates −63, −30, −2. Note that this general voxel location (within a 1 mm radius) was the most significant in both the gray and white matter SPMs representing a region where there is too much gray matter and too little white matter in the ALC patients. The mean for each group is represented by the black diamond symbols in each graph.

have also been observed in these patients, though hemispheric measures were not presented in the earlier report [6]. The regional differences in tissue distribution do not appear to strongly influence overall volumes of gray matter and white matter in these patients given that total white matter volume is not reduced disproportionate to brain size reduction in the ALC patients. There is only a trend towards a volume increase in gray matter in the ALC subjects relative to controls once brain size differences are controlled. Perhaps the subtle increase in total gray matter in ALC patients is disproportionately carried by a larger relative increase in gray matter specific to the perisylvian region in the left hemisphere. Taken together, these results provide evidence for local dysmorphology above and beyond the overall microcephaly that results from severe prenatal alcohol exposure.

As in our previous reports of brain morphology in ALC patients [6,7], the PEA subjects also displayed an abnormal pattern of tissue distribution revealed here with VBM. Notably, the pattern of results from gray matter SPMs in PEA patients relative to controls was spatially similar to that observed for the entire group of ALC patients and for the FAS patients compared to controls, but the statistical effect was much smaller. The FAS group without the PEA subjects appear to be more severely affected (i.e. larger clusters at the same statistical threshold), despite somewhat reduced statistical power with the reduced sample size. PEA patients are not as severely cognitively affected as the FAS patients [14]. Perhaps in a similar vein, their brain morphology is also less severely affected by the prenatal alcohol exposure. It should be noted, however, that statistical power was significantly reduced with only seven PEA patients, relative to the 21 ALC patients studied in the planned analyses. Thus, it is possible that with a larger sample larger differences in brain morphology would also be observed. Regardless, differences were observed in the PEA patients, again, illustrating that they do have brain dysmorphology in the absence of facial dysmorphology required for the diagnosis of FAS.

Strictly speaking, direct conclusions about the localization of abnormalities cannot be made with these data. That is, while left perisylvian cortices appear to be the most affected in the SPMs, one cannot conclude that other regions are completely unaffected by prenatal alcohol exposure. Nor can one conclude that the left perisylvian region is necessarily more affected than any other region. This is because the statistical significance of the difference in effect sizes in various regions of the brain has not been assessed in the VBM analyses. Other regions of the brain are probably affected beyond the overall microcephaly resultant from prenatal exposure to alcohol, though they are not apparent at the voxel threshold utilized for these analyses. Nonetheless, it can be confidently concluded from these results that the statistical distribution of effects related to prenatal alcohol exposure is most prominent in the perisylvian cortex, an anatomic region consistent with our *a priori* hypotheses.

The etiology of the abnormalities observed in the ALC patients cannot be directly assessed with MRI. However, the general location of gross dysmorphology in relatively lateral cortices and the tendency for ALC subjects to have too little white matter with too much gray matter lead to speculation regarding the cellular developmental processes which may have gone awry. Animal studies have shown that prenatal alcohol exposure during different periods of brain development can result in regional differences in cell

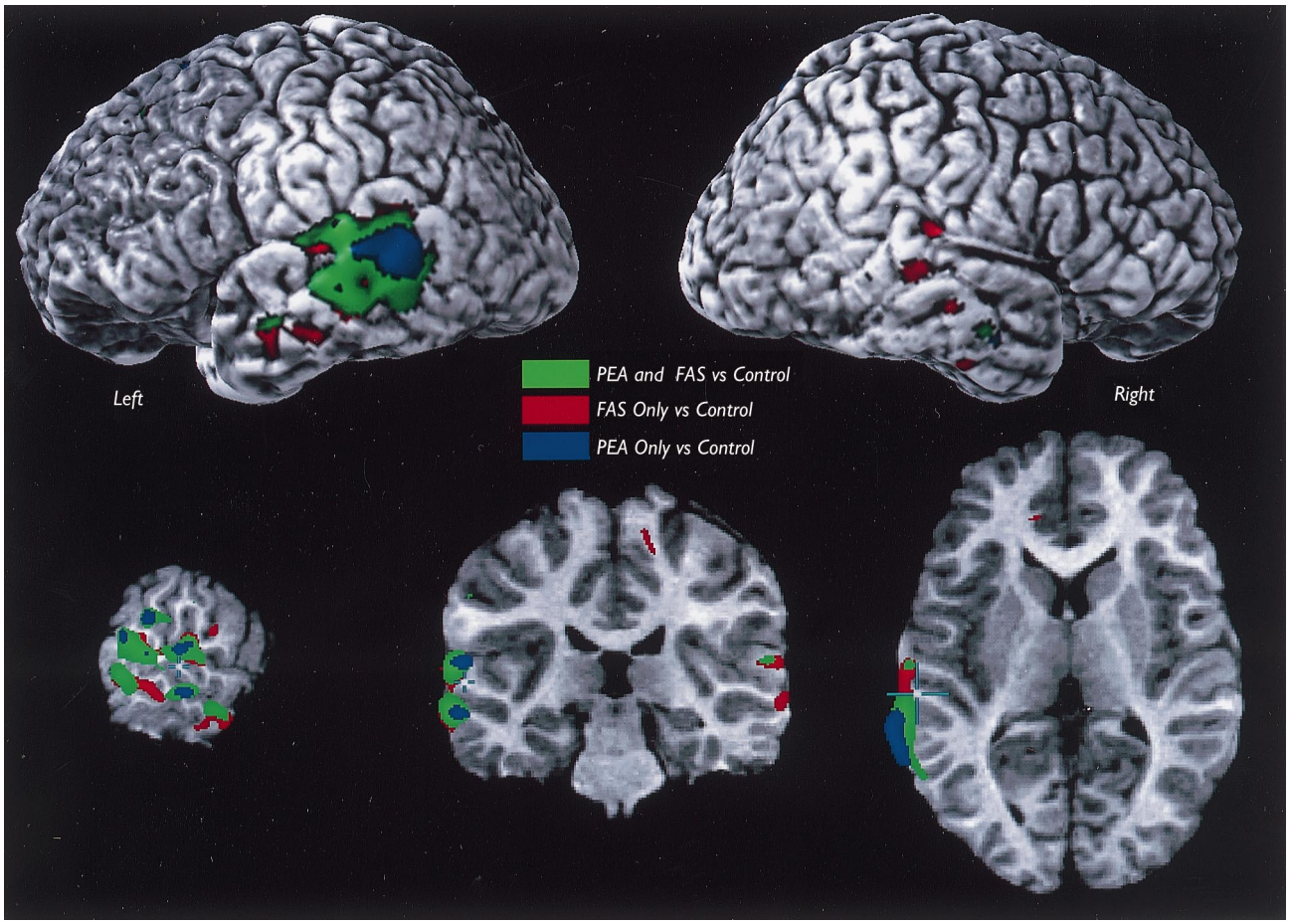

Fig. 7. Gray matter SPMs for the entire ALC group *vs* controls (shown in green; voxel threshold $p = 0.0001$, $\geqslant 50$ significant voxels), the 14 FAS patients *vs* controls (shown in red; voxel threshold $p = 0.0001$, $\geqslant 50$ significant voxels), and the seven PEA patients *vs* controls (shown in blue; voxel threshold $p = 0.001$, $\geqslant 50$ significant voxels) mapped onto the surface rendering of one individual's brain (top). The same SPMs are mapped onto three orthogonal slices of one individual subject's brain (bottom). Note the correspondence in the location of the clusters, for the three separate SPM analyses.

death depending on the timing of the exposure [26]. In addition to cell death, depending on the timing, alcohol can disrupt the division and proliferation of new cells, cell growth, and differentiation and migration patterns [27]. These cellular events might result in local abnormalities of gray matter observable with MRI. Regional glial cell abnormalities such as in aberrant myelinogenesis and neuroglial heterotopias are also prominent in animals prenatally exposed to alcohol, [28]. These cellular events could be related to the regionally variable reduction of white matter observed in the ALC subjects.

Less understood from human or animal research is the link between exposure to alcohol at a static point in embryogenesis, and the disruption of cellular events that occur much later in development. For example, myelination continues to occur in humans into the third decade of life and beyond [29], long after prenatal exposure to alcohol has ceased. Brain maturational changes, probably continued myelination, have been observed in humans *in vivo* using methods similar to those reported here [17,21,30]. Longitudinal MRI studies of maturation in individuals prenatally exposed to alcohol may help shed light on the long-term effects of alcohol and its interaction with developmental processes.

REFERENCES

1. Abel EL and Sokol RJ. *Alcohol Clin Exp Res* **15**, 514–524 (1991).
2. West JR, Chen WJ and Pantazis NJ. *Metab Brain Dis* **9**, 291–322 (1994).
3. Roebuck TM, Mattson SN and Riley EP. *Alcohol Clin Exp Res* **22**, 339–344 (1998).
4. Mattson SN, Riley EP, Sowell ER *et al. Alcohol Clin Exp Res* **20**, 1088–1093 (1996).
5. Swayze VW, Johnson VP, Hanson JW *et al. Pediatrics* **99**, 232–240 (1997).
6. Archibald SL, Fennema-Notestine C, Riley EP *et al. Dev Med Child Neurol* (In Press).
7. Sowell ER, Mattson SN, Thompson PM et al. Submitted.
8. Riley EP, Mattson SN, Sowell ER *et al. Alcohol Clin Exp Res* **19**, 1198–1202 (1995).
9. Riikonen R, Salonen I, Partanen K and Verho S. *Dev Med Child Neurol* **41**, 652–659 (1999).
10. Sowell ER, Jernigan TL, Mattson SN *et al. Alcohol Clin Exp Res* **20**, 31–34 (1996).
11. Aboitiz F, Scheibel AB and Zaidel E. *Brain* **115**, 1521–1541 (1992).

12. Abell F, Krams M, Ashburner J *et al. Neuroreport* **10**, 1647–1651 (1999).
13. Sowell ER, Levitt J, Thompson PM *et al. Am J Psychiatry* **157**, 1475–1484 (2000).
14. Mattson SN, Riley EP, Gramling L *et al. J Pediatr* **131**, 718–721 (1997).
15. Mattson SN, Riley EP, Gramling L *et al. Neuropsychology* **12**, 146–153 (1998).
16. Jones KL and Smith DW. *Lancet* **2**, 999–1001 (1973).
17. Sowell ER, Thompson PM, Holmes CJ *et al. Neuroimage* **9**, 587–597 (1999).
18. Evans AC, Kamber M, Collins DL and MacDonald D. An MRI-based probabilistic atlas of neuroanatomy. In: Shorvon SD, ed. *Magnetic Resonance Scanning and Epilepsy*. New York: Plenum; 1994, pp. 263–274.
19. Woods RP, Mazziotta JC and Cherry SR. *J Comp Assist Tomogr* **17**, 536–546 (1993).
20. Friston KJ, Holmes AP, Worsley KJ *et al. Human Brain Mapp* **2**, 189–210 (1995).
21. Sowell ER, Thompson PM, Holmes CJ *et al. Nature Neurosci* **2**, 859–861 (1999).
22. Bullmore E, Brammer M, Williams SC *et al. Magn Reson Med* **35**, 261–277 (1996).
23. Ashburner J and Friston KJ. *Neuroimage* **11**, 805–821 (2000).
24. Worsley KJ, Andermann M, Koulis T *et al. Hum Brain Mapp* **8**, 98–101 (1999).
25. Talairach J and Tournoux *P. Co-planar Stereotaxic Atlas of the Human Brain*. New York: Thieme; 1988.
26. Maier SE, Miller JA, Blackwell JM and West JR. *Alcohol Clin Exp Res* **23**, 726–734 (1999).
27. Guerri C. *Alcohol Clin Exp Res* **22**, 304–312 (1998).
28. Guerri C and Renau-Piqueras J. *Mol Neurobiol* **15**, 65–81 (1997).
29. Yakovlev PI and Lecours AR. In Minkowski A, ed. *Regional Development of the Brain in Early Life*. Oxford: Blackwell Scientific; 1967, pp. 30–70.
30. Paus T, Zijdenbos A, Worsley K *et al. Science* **283**, 1908–1911 (1999).

Acknowledgements: Funding Support: NCRR P41 RR13642, NINDS NS3753 (PI A.W.T.), NIAAA AA 10417 (PI E.P.R.), and AA 10820 (PI S.N.M.).